Hindawi Publishing Corporation
Mathematical Problems in Engineering
Volume 2014, Article ID 784731, 11 pages
http://dx.doi.org/10.1155/2014/784731

Research Article

Impedance-Based Cable Force Monitoring in Tendon-Anchorage Using Portable PZT-Interface Technique

Thanh-Canh Huynh and Jeong-Tae Kim

Department of Ocean Engineering, Pukyong National University, Daeyeon-dong, Nam-gu, Busan 608-737, Republic of Korea

Correspondence should be addressed to Jeong-Tae Kim; idis@pknu.ac.kr

Received 30 December 2013; Accepted 5 March 2014; Published 30 March 2014

Academic Editor: Ting-Hua Yi

In this paper, a portable PZT interface for tension force monitoring in the cable-anchorage subsystem is developed. Firstly, the theoretical background of the impedance-based method is presented. A few damage evaluation approaches are outlined to quantify the variation of impedance signatures. Secondly, a portable PZT interface is designed to monitor impedance signatures from the cable-anchorage subsystem. One degree-of-freedom analytical model of the PZT interface is established to explain how to represent the loss of cable force from the change in the electromechanical impedance of the PZT interface as well as reducing the sensitive frequency band by implementing the interface device. Finally, the applicability of the proposed PZT-interface technique is experimentally evaluated for cable force-loss monitoring in a lab-scaled test structure.

1. Introduction

Recently, structural health monitoring (SHM) has been spotlighted in aerospace and civil infrastructures [1–3]. Among a variety of SHM studies, many researchers have focused on monitoring prestressed structures by using global and local dynamic characteristics [4–10]. For global methods, the acceleration response of low frequency range has been usually utilized to monitor the change in structural characteristics. However, the low-frequency vibration responses are not very sensitive to local prestress loss occurring in cable-anchorage subsystem. For local methods, on the other hand, the electromechanical (EM) impedance response of a high frequency range has been very promising to monitor small incipient change of structural characteristics.

The impedance-based method was first proposed by Liang et al. [11]. Since then, many researchers have improved the method and applied it into various damage detection problems such as pipeline system [12], thin circular plate [13], concrete beam and frame [14, 15], plate girder bridge [16], and bolted connection [17]. The method utilizes the EM impedance of a coupled PZT-structure system to detect the change in structural characteristics at local critical region. For damage monitoring, the change in impedance is usually quantified by the statistical pattern recognition or simply by the impedance shift at resonance [8, 13, 17–19].

Recently, Kim et al. [8] applied the impedance-based method for prestress-loss monitoring in tendon-anchorage connection by detecting the change in pattern of the impedance responses at the anchorage. Although the method has shown the excellent performance to detect prestress loss in tendon anchorage, it still has a few limitations for practical applications. Firstly, the effective frequency band which is sensitive to the variation of prestress force could be very significant, even above 800 kHz for a monotendon anchorage [8], as shown in Figure 1. In this case, a high performance impedance analyzer is needed to capture signals from such a high frequency range. Due to its bulky size, this device is not convenient to be implemented out of laboratory. Moreover, the price associated with the instrument system is very costly. To overcome these disadvantages, many efforts have been carried out by adopting wireless impedance device [9, 20]. In order to apply the new approach, however, the measurable frequency range of 10 kHz–100 kHz of the wireless sensors should be dealt appropriately for impedance measurement as well as feature extraction. Secondly, the impedance frequency bands which are sensitive to prestress loss should be predetermined before employing the impedance-based method for

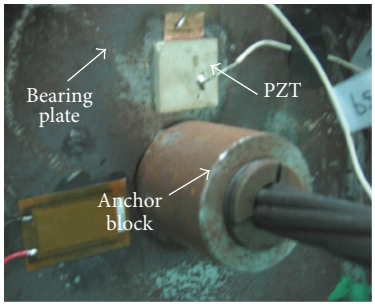

(a) Tendon-anchorage connection

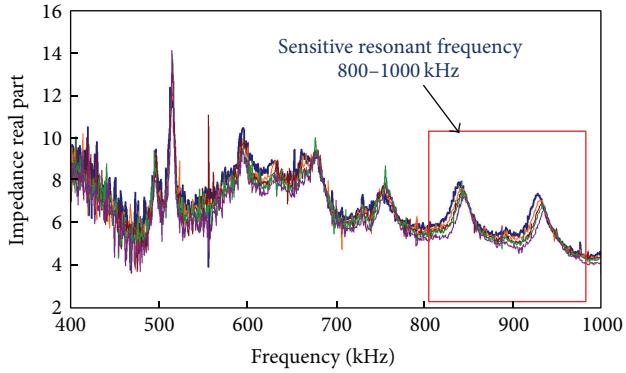

(b) Variation of EM impedance

FIGURE 1: Prestress-loss monitoring by anchorage's impedance [8].

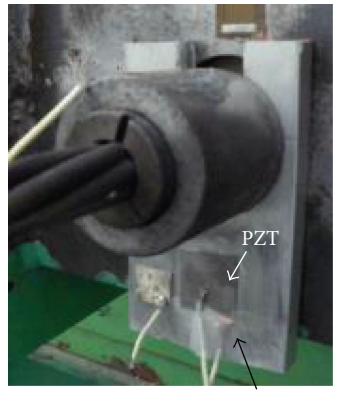

(a) PZT-interface in anchorage

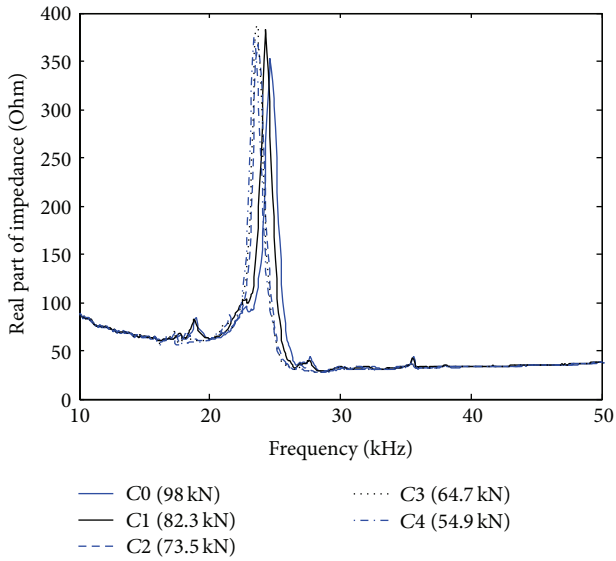

(b) Impedance signatures under various prestress forces

FIGURE 2: Prestress-loss monitoring using PZT-interface [21].

the damage detection job. Generally, the effective frequency range is varied dependent on target structures and usually determined by trial and error. This causes difficulty when dealing with real structures since the effective frequency range is almost unknown and may take much effort to obtain it by trial and error.

In order to overcome the above-mentioned limitations, Nguyen and Kim [21] proposed an impedance-sensitive PZT interface for monitoring prestress loss in tendon-anchorage subsystem. The interface device is a thin aluminum plate equipped with a PZT patch. As shown in Figure 2(a), the PZT-interface is partly clamped at one end by a bearing plate and an anchor block and freely vibrated at another end. The implementation of the PZT interface was successful in indicating various prestress losses in the tendon-anchorage connection. Also, the sensitive frequency range to prestress loss was reduced to below 100 kHz (Figure 2(b)) which was measurable by a wireless impedance sensor system. However, this design of PZT interface must be installed during the construction of the cable-anchorage subsystem. So it is impossible to apply it into existing cable-supported structures. Also, the presence of this aluminum interface device between anchor and bearing plate may reduce bearing capacity of cable-anchorage system due to its low stiffness.

In order to overcome the drawbacks of the newly designed interface device, a portable PZT interface is developed for the impedance-based cable force monitoring in tendon anchorage. Firstly, the principle of the impedance-based monitoring technique is presented. A few damage evaluation approaches are outlined to quantify the variation of impedance signatures. Secondly, a portable PZT interface is designed for monitoring impedance signatures from postinstallation into existing cable-anchorage connections. A one degree-of-freedom analytical model of PZT interface is established to explain how to represent the loss of cable force from the change in the EM impedance of PZT interface as well as reducing the sensitive frequency band by implementing the interface device. Finally, the applicability of the proposed PZT-interface technique is evaluated experimentally for cable force-loss monitoring in a lab-scaled test structure.

2. Impedance-Based Monitoring Technique

2.1. Electromechanical Impedance. To monitor structural change, a piezoelectric material (e.g., PZT) is surface bonded to structure at examined region. The interaction between

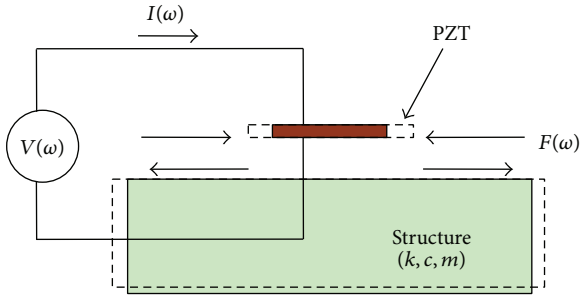

Figure 3: Model of coupling interaction between PZT transducer and structure.

the PZT and the structure is simply explained by 1D free-body diagram of PZT-structure system as shown in Figure 3. Due to inverse piezoelectric effect, an input harmonic voltage $V(\omega)$ induces a deformation of PZT. Because the PZT is bonded to the structure, a force $F(\omega)$ against that deformation is induced into the structure and the PZT as well. For 1 dof system, the structural mechanical impedance of the host structure $Z_s(\omega)$ is obtained by the ratio of force $F(\omega)$ to velocity $\dot{u}(\omega)$ as follows [11]:

$$Z_s(\omega) = \frac{F(\omega)}{\dot{u}(\omega)} = c + m\frac{\omega^2 - \omega_n^2}{\omega} i, \tag{1}$$

where c and m are the damping coefficient and the mass of the structure, respectively; ω_n is the angular natural frequency of the structure; and ω is the angular frequency of the excitation voltage. As shown in (1), the structural mechanical impedance is a function of mass, damping, and stiffness (i.e., stiffness is introduced from natural frequency, $k = m\omega_n^2$). Thus, the change in structural parameters can be represented by the change in the structural mechanical impedance.

In practice, the electric current $I(\omega)$ is measured and then it is utilized to calculate the EM impedance as follows [11, 22]:

$$Z(\omega) = \frac{V}{I} = \left\{ i\omega \frac{w_a l_a}{t_a} \left[\hat{\varepsilon}_{33}^T - \frac{1}{Z_a(\omega)/Z_s(\omega) + 1} d_{3x}^2 \hat{Y}_{xx}^E \right] \right\}^{-1}, \tag{2}$$

where $\hat{Y}_{xx}^E = (1 + i\eta) Y_{xx}^E$ is the complex Young's modulus of the PZT patch at zero electric field; $\hat{\varepsilon}_{xx}^T = (1 - i\delta)\varepsilon_{xx}^T$ is the complex dielectric constant at zero stress; d_{3x} is the piezoelectric coupling constant in x-direction at zero stress; $k = \omega\sqrt{\rho/\hat{Y}_{xx}^E}$ is the wave number where ρ is the mass density of the PZT patch; and w_a, l_a, and t_a are the width, length, and thickness of the piezoelectric transducer, respectively. The parameters η and δ are structural damping loss factor and dielectric loss factor of piezoelectric material, respectively. As shown in (2), the EM impedance, $Z(\omega)$, is a combining function of the mechanical impedance of the host structure, $Z_s(\omega)$, and that of the piezoelectric patch, $Z_a(\omega)$. Therefore, the change in structural parameters (k,m, c) can be represented by the change in the EM impedance.

For damage monitoring using the impedance-based method, the frequency range which should be utilized is an important issue. The frequency band should be selected appropriately in order to realize the structural change in the EM impedance. Generally, if the excitation frequency is not identical to the natural frequency of the structure (i.e., $\omega \neq \omega_n$), the structural mechanical impedance takes the full term of (1). In this case, the impedance of the structure is very significant compared with the mechanical impedance of the PZT (i.e., $Z_s(\omega) \gg Z_a(\omega)$). As a result, the term $Z_a(\omega)/Z_s(\omega)$ is neglected and the EM impedance is approximated as

$$Z(\omega) \approx \left\{ i\omega \frac{w_a l_a}{t_a} \left[\varepsilon_{33}^T - d_{3x}^2 \hat{Y}_{xx}^E \right] \right\}^{-1}. \tag{3}$$

In (3), the contribution of the structural mechanical impedance to the EM impedance is filtered out. Therefore, the structural change may not be identified sensitively by the EM impedance. On the other hand, if PZT sensor is excited by a frequency matching with the natural frequency of the structure (i.e., $\omega = \omega_n$), and the structural mechanical impedance takes only the term of damping coefficient (i.e., $Z_s(\omega) = c$). Therefore, the structural impedance for that frequency is comparable with the mechanical impedance of the PZT, and the EM impedance is expressed as

$$Z(\omega) = \left\{ i\omega \frac{w_a l_a}{t_a} \left[\varepsilon_{33}^T - \frac{1}{Z_a/c + 1} d_{3x}^2 \hat{Y}_{xx}^E \right] \right\}^{-1}. \tag{4}$$

In (4), the contribution of the structural mechanical impedance to the EM impedance is the damping coefficient c. This contribution causes resonant response in the EM impedance signature at the correspondent frequency. In other words, the EM impedance at resonance represents not only the modal damping but also the natural frequency of the structure. Therefore, the structural change could be identified sensitively by the change in the EM impedance at a resonant frequency.

2.2. Damage Evaluation Approach

2.2.1. Root Mean Square Deviation. To quantify the change in the EM impedance, the root mean square deviation (RMSD) index is utilized [18]. RMSD index is calculated as

$$\mathrm{RMSD}(Z, Z^*) = \sqrt{\frac{\sum_{i=1}^N \left[Z^*(\omega_i) - Z(\omega_i) \right]^2}{\sum_{i=1}^N \left[Z(\omega_i) \right]^2}}, \tag{5}$$

where $Z(\omega_i)$ and $Z^*(\omega_i)$ are the impedances measured before and after damage for the ith frequency, respectively, and N denotes the number of frequency points in the sweep.

Basically, the RMSD is equal to 0 if no damage occurs and larger than 0 if damage occurs. However, due to experimental and environmental errors, the RMSD may be larger than 0 although damage does not occur. To deal with the uncertain conditions, the control chart analysis is used for decision-making out of RMSD values. The upper control limit of

the RMSD (UCL_{RMSD}) is adopted for alarming damage occurrence as follows:

$$UCL_{RMSD} = \mu_{RMSD} + 3\sigma_{RMSD}, \tag{6}$$

where μ_{RMSD} and σ_{RMSD} are mean and standard deviation of RMSD data set at undamaged condition, respectively. In (6), the UCL_{RMSD} is determined by three standard deviations of the mean, which is corresponding to 99.7% confidence level. The calculation of the UCL_{RMSD} is outlined in three steps: firstly, n impedance signals are measured at undamaged condition; secondly, RMSD values for n impedance signals are computed by (5), and then a set of RMSD values is obtained; and finally, the UCL_{RMSD} is calculated using (6). The occurrence of damage is indicated when the RMSD values are larger than the control limit. Otherwise, there is no indication of damage occurrence.

2.2.2. Correlation Coefficient Deviation. The correlation coefficient deviation (CCD) index can also be used to quantify the change of the whole impedance signatures [13]. The CCD index is calculated as follows:

$$CCD = 1 - \frac{1}{\sigma_Z \sigma_Z^*} E\left\{\left[\mathrm{Re}\left(Z_i\right) - \mathrm{Re}\left(\bar{Z}\right)\right] \times \left[\mathrm{Re}\left(Z_i^*\right) - \mathrm{Re}\left(\bar{Z}^*\right)\right]\right\}, \tag{7}$$

where $E[\cdot]$ is the expectation operation; $\mathrm{Re}(Z_i)$ signifies the real parts of the EM impedances of the ith frequency before and after damage; $\mathrm{Re}(\bar{Z})$ signifies the mean values of impedance signatures (real part) before and after damage; and σ_Z signifies the standard deviation values of impedance signatures before and after damage. Note that the asterisk (*) denotes the damaged state.

Similarly, the upper control limit of the CCD (UCL_{CCD}) with 99.7% confidence level is computed to deal with the experimental and environmental errors, as follows:

$$UCL_{CCD} = \mu_{CCD} + 3\sigma_{CCD}, \tag{8}$$

where μ_{CCD} and σ_{CCD} are mean and standard deviation of CCD data set at undamaged condition, respectively. The calculation of the UCL_{CCD} is also outlined in three steps: firstly, n impedance signals are measured at undamaged condition; secondly, CCD values for n impedance signals are computed by (7), then a set of CCD values is obtained; and finally, the UCL_{CCD} is calculated using (8). When the CCD values are larger than the UCL_{CCD}, the occurrence of damage is alarmed. Otherwise, there is no warning sign of damage occurrence.

3. Portable PZT Interface for Impedance-Based Monitoring

3.1. Cable Force Monitoring by Impedance Response of Bearing Plate. A system of tendon anchorage under prestress force can be modeled by connection components (i.e., bearing plate, anchor block, and tendon) and contact forces in equilibrium condition, as shown in Figure 4(a). Prestress force is modeled by tendon force acting on the anchor block and transformed to contact pressure and bearing stress in the interface of anchor block and bearing plate. According to contact mechanism [23], the interaction in the contact interface can be simplified by two-dimensional damping and spring stiffness in normal and transverse axes, as shown in Figure 4(b). Basically, the interfacial spring stiffness and damping values represent the amount of contact pressure and stress field acting at the interface. In the previous study by Ritdumrongkul et al. [24], it was reported that the variation of interfacial stiffness and damping parameters is associated with the variation of contact pressure which is generated from bolt torque. Hence, the variation of tendon force can be treated as the variation of those structural parameters at the contact interface.

On the other hand, the change in the structural contact parameters can be identified sensitively by the change in the EM impedance at a resonant frequency, and an approach for cable force-loss monitoring is conducted by examining the EM impedance of anchorage. Due to that, the bearing plate is relatively more elastically deformable than the anchor block (i.e., assuming the anchor block as rigid body), and it is easier to capture the change in the structural contact parameters if the PZT patch is attached on the bearing plate, as shown in Figure 4(b). The main idea is that the EM impedance of the bearing plate is monitored to detect the change in the structural parameters at the contact interface, since these parameters represent the contact pressure (bearing stress) or tendon force.

Based on the analytical models of the interaction between piezoelectric patch and host structure [21, 22, 25], the bearing plate and the PZT patch are simply modeled as 1 dof system by bearing plate's mass (m^b), bearing plate's stiffness and damping (k^b, c^b), contact stiffness (k_1^c, k_2^c), and contact damping (c_2^c, c_2^c), as shown in Figure 4(c). For simplification, the series model is selected since the bearing plate is the target structure and the contact parameters are considered as the boundary conditions, as schematized in Figure 4(b).

The equivalent structural stiffness $(k_e)^A$ of the simplified model can be computed as

$$\left(k_e\right)^A = \frac{\left(k_1^c + k_2^c\right)k^b}{\left(k_1^c + k_2^c\right) + k^b} = \frac{k^c k^b}{k^c + k^b}, \tag{9}$$

where $k^c = k_1^c + k_2^c$ is the total contact stiffness; suppose $\alpha = k^b/k^c$ is the ratio of the bearing plate's stiffness to the total contact stiffness; then the equivalent structural stiffness is rewritten as follows:

$$\left(k_e\right)^A = \frac{\alpha k^c}{1+\alpha} = \gamma k^c \quad \text{where } \gamma = \frac{\alpha}{(1+\alpha)}. \tag{10}$$

It is worth noting that for cable-supported structures, the bearing plate's stiffness k^b and the total contact stiffness k^c are very considerable resulting in an enormous value of the equivalent structural stiffness. Consequently, the natural frequency of the system would be significantly high. Figure 1 illustrates the experimental setup and monitoring

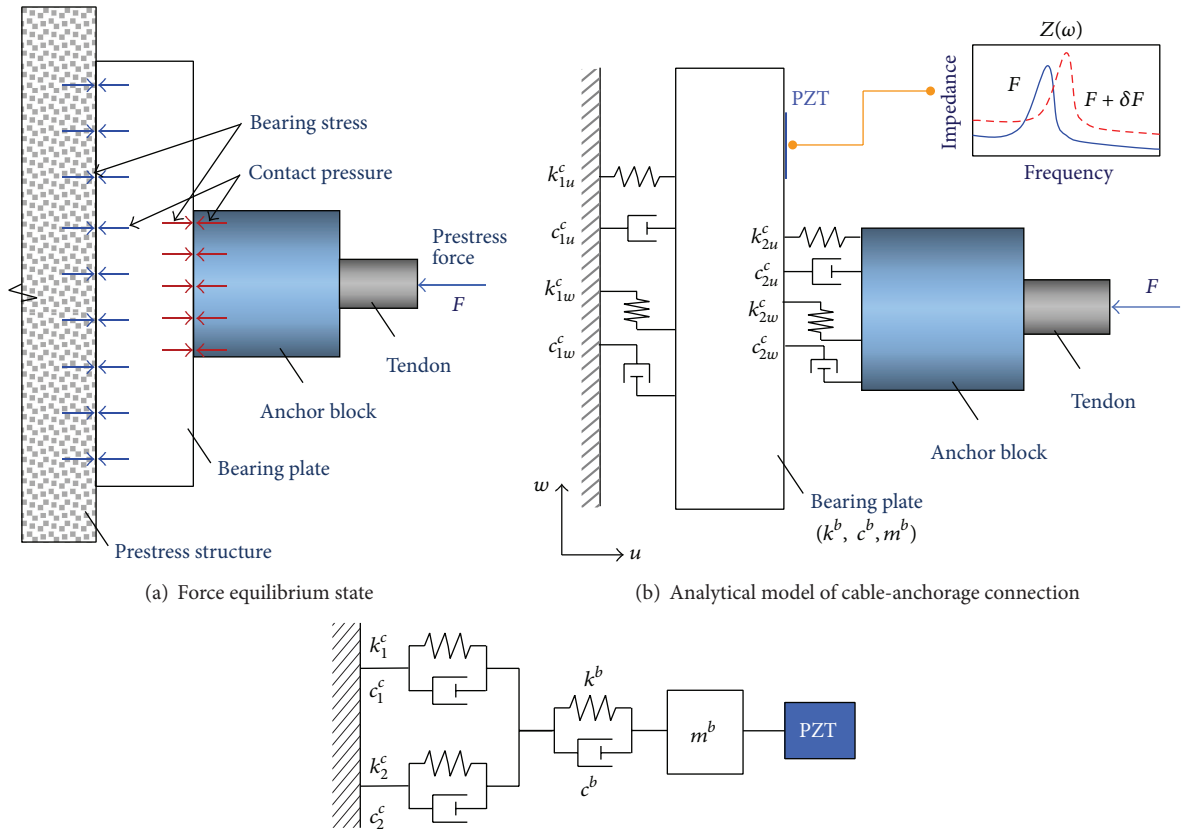

(a) Force equilibrium state

(b) Analytical model of cable-anchorage connection

(c) 1 dof model of bearing plate equipped with a PZT patch

FIGURE 4: Schematic of cable force monitoring by bearing plate's impedance.

results carried out by Kim et al. [8] on a lab-scale tendon anchorage. As shown in the figure, the EM impedance of the anchorage varied according to tendon force loss. However, the impedance response must be monitored in a very high resonant frequency range, above 800 kHz in that study. The experimental result proves that if the PZT is bonded at a very stiff region, the resonant response of the structure must be obtained at a very high frequency excitation.

3.2. Portable PZT Interface for Impedance-Based Monitoring. In order to reduce the high resonant frequency and deal with wireless impedance measurement, a PZT interface was given by Nguyen and Kim [21], as previously described in Section 1. The drawbacks of this PZT-interface design are preinstalled in the construction and affecting the bearing capacity of the cable-anchorage subsystem. In consideration of these disadvantages for the impedance-based cable force monitoring, a portable PZT interface is proposed as shown in Figure 5(a). The interface device is a thin-walled beam-like member with a PZT patch mounted on it. A partial free surface in the bottom of the interface is intentionally designed to make the PZT patch freely vibrating when being mounted on the bearing plate.

Figure 5(b) schematizes an analytical model of cable-anchorage connection with equivalent structural parameters at contact boundary surfaces. Since the EM impedance technique is very sensitive to structural changes in near field boundary condition, any change in structural variables due to cable force loss would lead to the change in the EM impedance response of PZT interface. By this way, the loss of cable force can be monitored by the portable PZT interface. The primary advantages of this interface design are its mobility and its adaptability to be applied in any existing cable-anchorage connections.

As shown in Figure 5(c), the PZT interface is simply modeled as 1 dof system by PZT interface's mass (m^i), PZT interface's stiffness and damping (k^i,c^i), contact stiffness (k_1^c, k_2^c), and contact damping (c_1^c, c_2^c) [21, 22, 25]. The equivalent structural stiffness $(k_e)^B$ is then computed as

$$(k_e)^B = \frac{\gamma k^c k^i}{\gamma k^c + k^i}. \tag{11}$$

Suppose $\beta = k_i/k_c$ is the ratio of the PZT interface's stiffness to the total contact stiffness; the equivalent structural stiffness is rewritten as follows:

$$(k_e)^B = \frac{\beta\gamma k^c}{\beta + \gamma}. \tag{12}$$

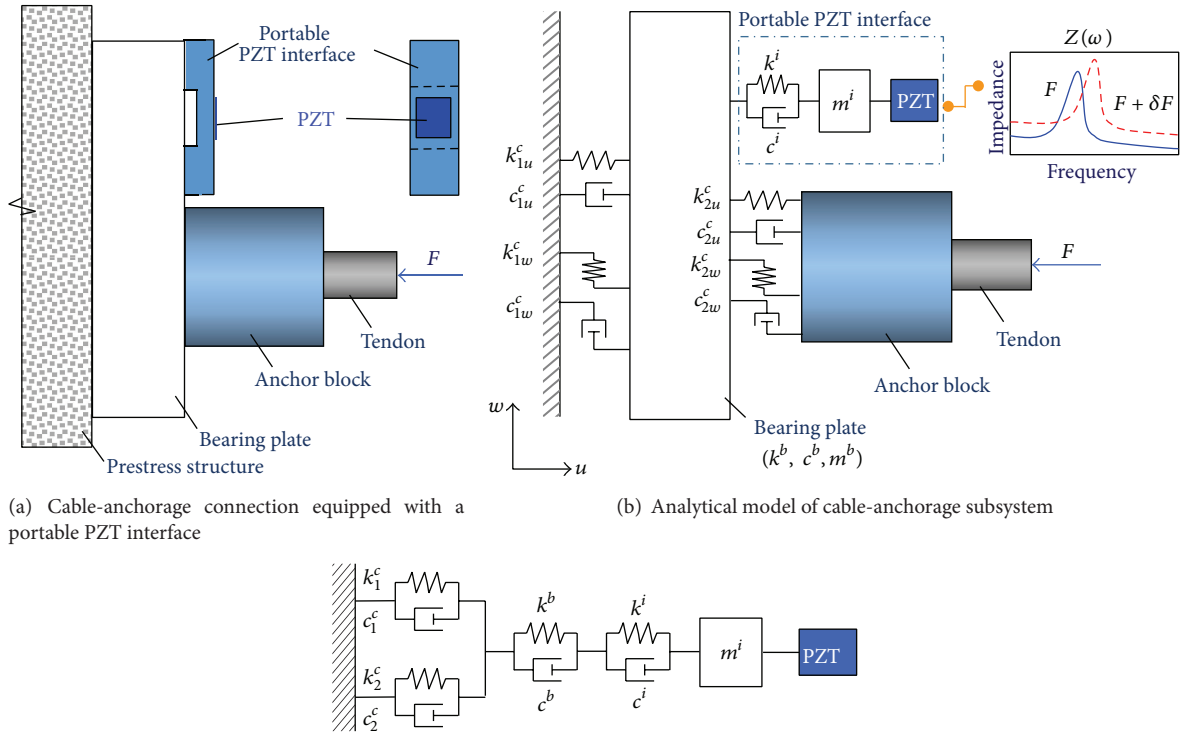

(a) Cable-anchorage connection equipped with a portable PZT interface

(b) Analytical model of cable-anchorage subsystem

(c) 1 dof model of portable PZT interface

Figure 5: Schematic of cable force monitoring by portable PZT interface's impedance.

Substituting (12) into (10) leads to the ratio of the equivalent stiffness of the PZT interface $(k_e)^A$ to that of the bearing plate $(k_e)^B$ as follows:

$$\frac{(k_e)^B}{(k_e)^A} = \frac{\beta}{\gamma+\beta} = \frac{1}{\gamma/\beta+1} < \frac{1}{\gamma/\beta} = \frac{\beta}{\gamma}. \tag{13}$$

If the PZT interface's stiffness k^i is much smaller than the bearing plate's stiffness k^b ($\beta \ll \alpha$), then $\beta \ll \gamma$; and therefore the equivalent structural stiffness of PZT-interface system will become much smaller than that of bearing plate system, $(k_e)^B \ll (k_e)^A$ according to (13). Assume the mass of the PZT interface (m^i) is comparable with that of the bearing plate (m^b); the natural frequency of the PZT-interface system would be significantly reduced. It should be experimentally proved that the effective frequency range of the EM impedance is smaller than 100 kHz by implementing a portable aluminum PZT interface.

4. Experimental Evaluation of Portable PZT Interface for Cable Force Monitoring

4.1. Experimental Setup. An experiment was carried out for a lab-scale cable-anchorage system to validate the implementation of proposed PZT interface for the impedance-based cable force monitoring. As shown in Figure 6, a cable in length of 6.4 m was anchored by two bearing plates at two ends; and tension force was introduced into the cable by a

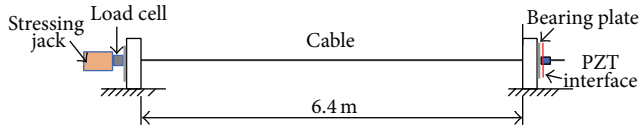

Figure 6: Schematic of cable-anchorage system.

stressing jack. A load cell was installed at one cable anchorage to measure the actual cable force. The experimental setup on tendon anchorage is also described in Figure 7. An aluminum interface equipped with a PZT-5A patch (Lead Zirconate Titanate) was installed on the bearing plate of tendon-anchorage connection (Figure 7(b)). The PZT sensor was excited by a harmonic excitation voltage with 1 V amplitude, and the impedance signature was measured by a commercial impedance analyzer HIOKI 3532 (Figure 7(c)). The cable was first pretensioned to $T0 = 49.5$ kN which was considered as the healthy state. For cable damage simulation, the tension force was reduced to $T1 = 39.2$ kN, $T2 = 29.4$ kN, and $T3 = 19.6$ kN, as listed in Table 1. For each damage case, five repeated measurements were conducted. During the measurements, the stressing jack was removed from the cable-anchorage system to avoid the influence of the jack weight on the actual cable force. Although the upper control limit could be used to deal with the experimental and environmental errors, not all environmental errors could be excluded such as temperature change. In the scope of

(a) Cable anchorage

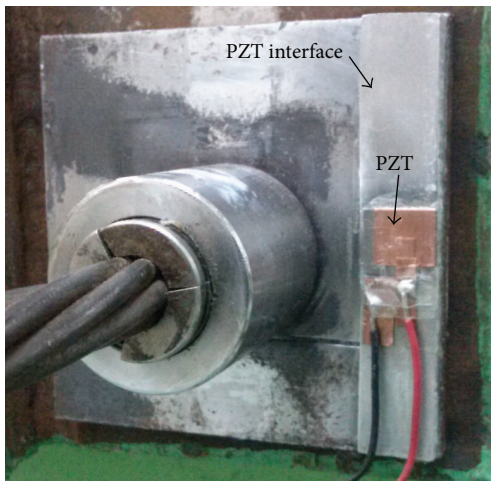

(b) PZT interface

(c) Impedance analyser

Figure 7: Experimental setup for impedance-based cable force monitoring.

Table 1: Cable force-loss monitoring by frequency shift.

Case	Cable force		Resonant frequency			
	T (kN)	ΔT (%)	f_1 (kHz)	Δf_1 (%)	f_2 (kHz)	Δf_2 (%)
$T0$	49.05	0	19.63	0	82.23	0
$T1$	39.2	−20.1	19.63	0	82.15	−0.1
$T2$	29.4	−40.1	19.57	−0.3	82.03	−0.2
$T3$	19.6	−60	19.53	−0.5	—	—

this study, therefore, room temperature was kept as close as constant of 23-24°C by air conditioners during the tests.

4.2. Cable Force versus Impedance Response. As stated previously, the primary motivation to invent the interfacing device is to fulfill the specification of wireless impedance sensors. According to the specification of wireless impedance devices [9, 20], the frequency sweep should be within 10–100 kHz to ensure the accuracy of impedance measurement as well as feature extraction. Therefore, the frequency range 10–100 kHz was examined to evaluate the feasibility of the portable PZT interface on cable force monitoring using wireless technology. In general, real part of EM impedance contains much more information of structural behaviors than imaginary part [18, 26]. Hence, real part of impedance response was examined for tendon force-loss monitoring.

Figure 8(a) shows real impedance signatures of the PZT interface in the wide frequency range 10 kHz–100 kHz (901 interval points) for the healthy state $T0$ and three damage cases $T1$ – $-T3$. From this figure, two resonant frequency bands of 15–25 kHz (501 interval points) and 75–95 kHz (501 interval points) are taken into account, as respectively shown in Figures 8(b) and 8(c). It is observed that the impedance signatures in the resonant bands of 15–25 kHz and 75–95 kHz are sensitively varied when cable force decreases. This implies that the contribution of the structural impedance to the EM impedance is considerable in the two resonant frequency ranges, which are explained in (4). By contrast, the impedance signatures in the nonresonant region 25–75 kHz are almost unchanged according to cable force loss. That is because impedance signatures in those

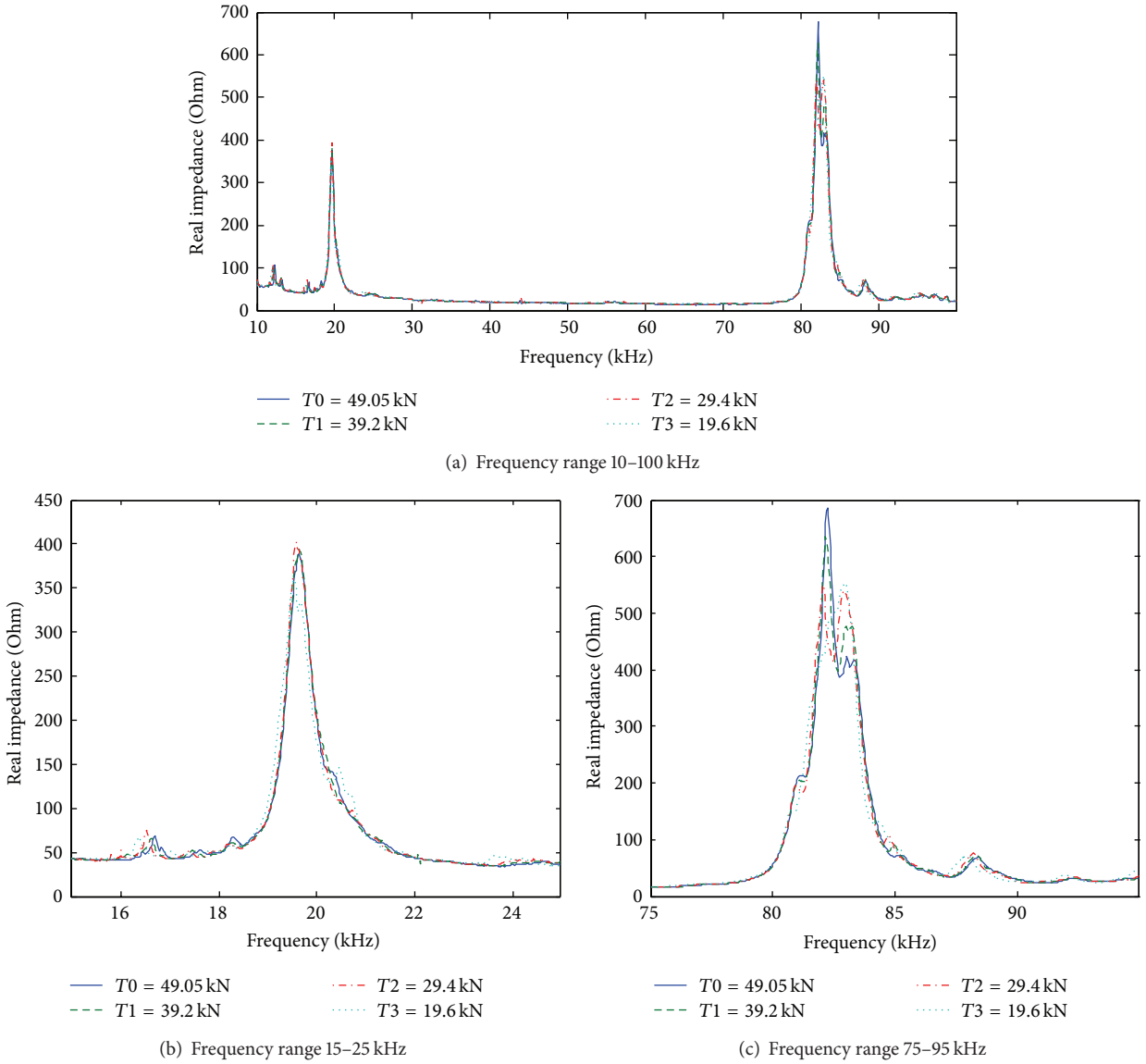

(a) Frequency range 10–100 kHz

(b) Frequency range 15–25 kHz

(c) Frequency range 75–95 kHz

Figure 8: Impedance signatures of PZT interface under various cable forces.

ranges are associated with only PZT properties as clarified in (3).

The resonant frequencies tend to shift left according to the decrement of cable force (Figures 8(b) and 8(c)). This indicates that modal stiffness of the whole system including the PZT interface and bearing plate is decreased with the reduction of cable force. For the four tension levels, the resonant frequencies corresponding to two resonant bands are outlined in Table 1. It is found that the frequency shift is very small, not greater than 0.5% for the first resonant frequency (f_1) and 0.2% for the second one (f_2). For the damaged case $T3$, moreover, the second resonant frequency could not be identified. Therefore, the frequency shift is not reliable to quantify the impedance variation in this study.

Generally, the CCD is sensitive to the horizontal shift and less sensitive to the vertical shift of the impedance signature while the RMSD is sensitive to both. As observed in Figure 8, the cable force loss causes not only the vertical shift but also the horizontal shift of the impedance response. Therefore, both RMSD and CCD indices are examined for four tension levels. The cable force monitoring results are summarized in Table 1. Figures 9 and 10, respectively, show the RMSD and CCD indices calculated according to the increment of cable force loss for the wide frequency band (i.e., 10–100 kHz) and the narrow ones (i.e., 15–25 kHz and 75–95 kHz). It is worthy to note that the RMSD and CCD indices are the mean values obtained from five repeated measurements of each damage case.

Both RMSD and CCD indices increase proportionally with the reduction of cable force. Obviously, RMSD and CCD indices of the wide frequency range of 10–100 kHz show good indication of cable force loss as the sensitive frequency range of 75–95 kHz and even better than that of 15–25 kHz. It is found that RMSD indices are higher than

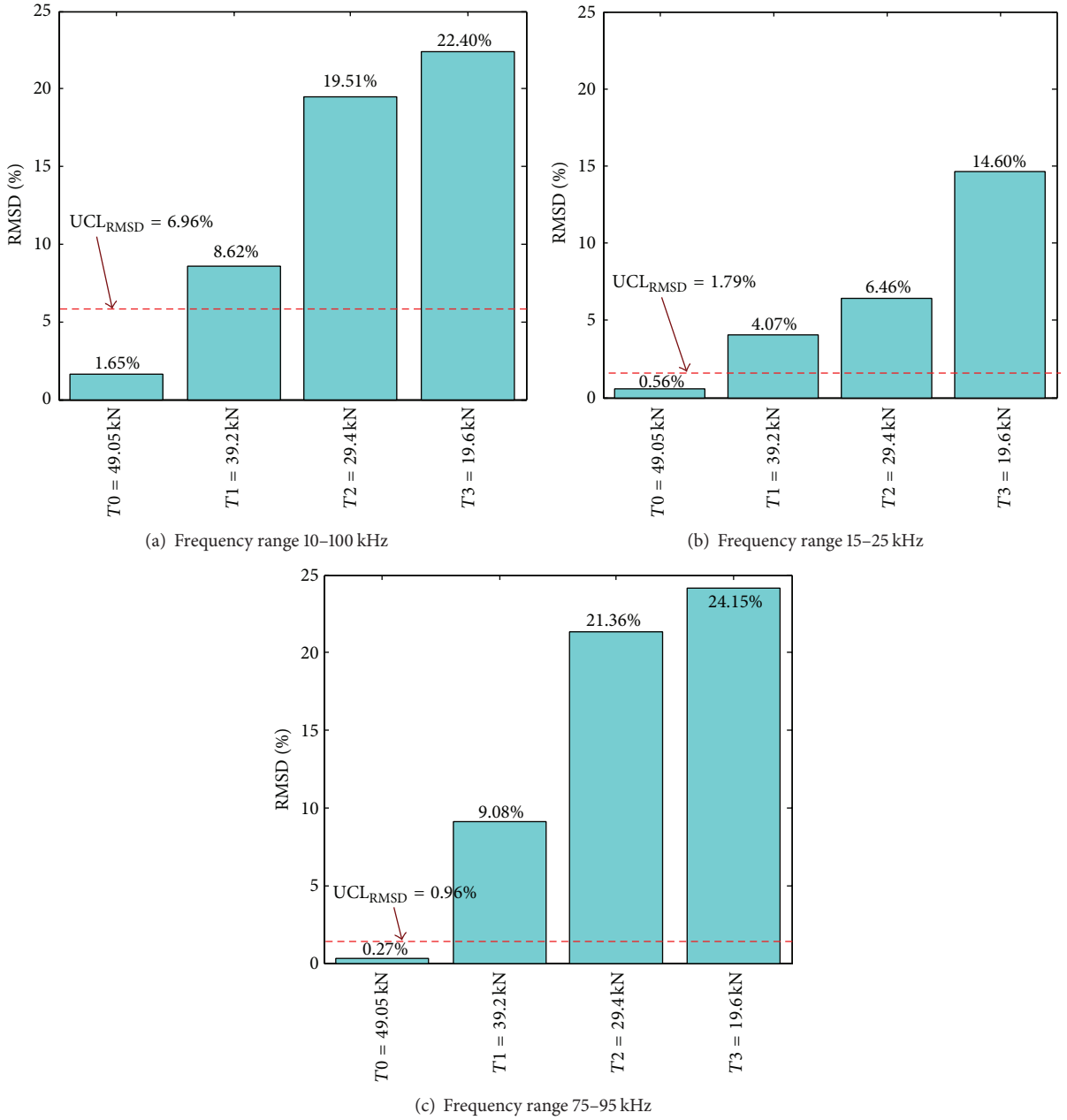

(a) Frequency range 10–100 kHz

(b) Frequency range 15–25 kHz

(c) Frequency range 75–95 kHz

Figure 9: Cable force-loss monitoring by RMSD index.

CCD indices for all considered frequency bands (i.e., 10–100 kHz, 15–25 kHz, and 75–95 kHz). This result indicates that the RMSD damage indicator can better indicate the change in impedance response due to the loss of cable force.

By implementing the proposed PZT interface, the good results of cable force monitoring were achieved not only for the sensitive frequency range but also for the whole measurable frequency band of 10–100 kHz.

5. Concluding Remarks

In this study, a portable PZT interface was developed to deal with the problems of the frequency range selection for the impedance-based cable force monitoring in tendon anchorage. Firstly, the principle of the impedance-based monitoring method was presented. A few damage evaluation approaches were outlined to quantify the variation of impedance signatures. Secondly, a portable PZT interface was designed for monitoring impedance signatures from postinstallation into existing cable-anchorage members. A one degree-of-freedom analytical model of PZT interface was established to explain how to represent the loss of cable force from the change in the electromechanical (EM) impedance of PZT interface as well as reducing the sensitive frequency band by implementing the interface device. Finally, the applicability of the proposed PZT-interface technique was experimentally

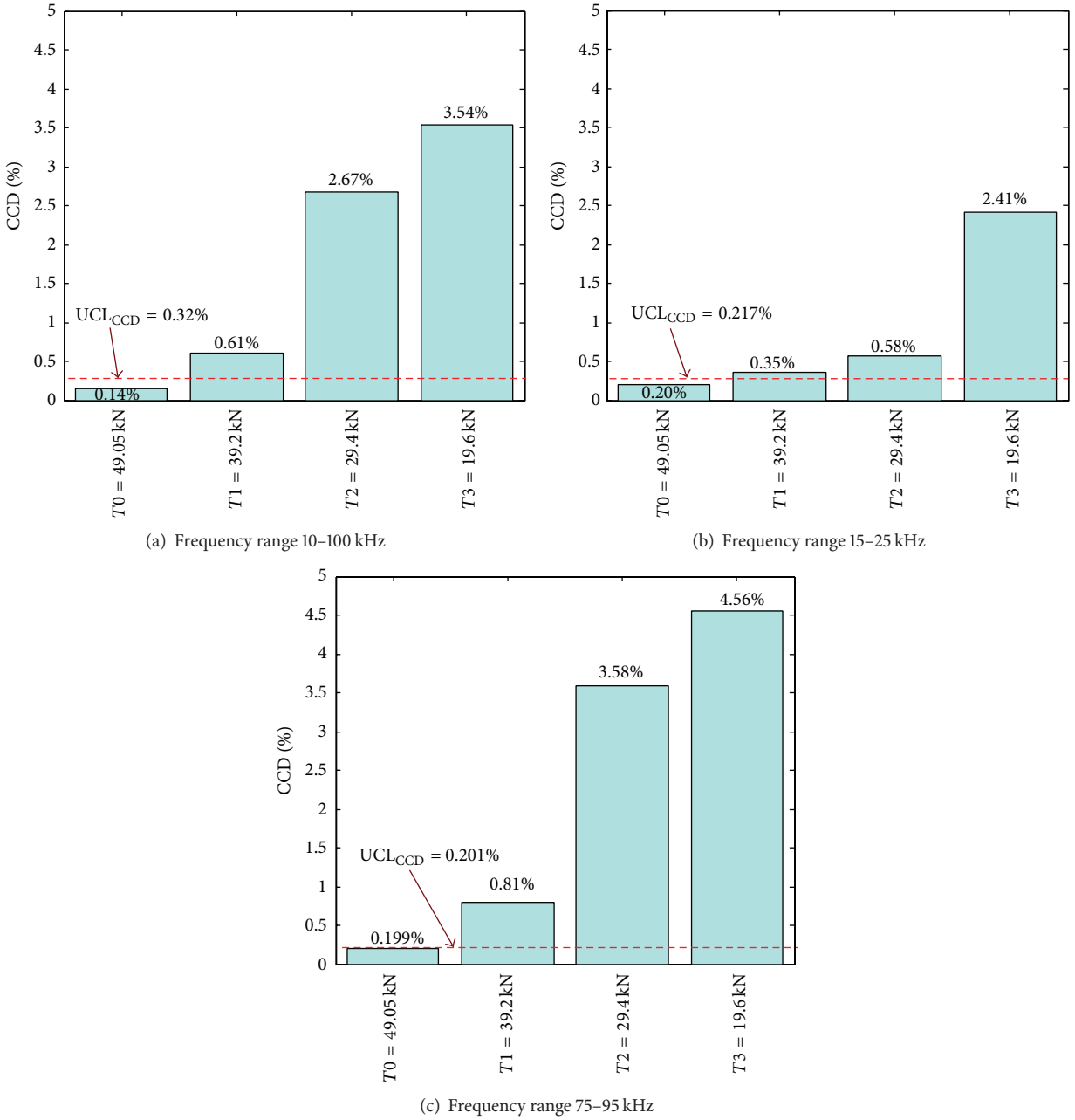

(a) Frequency range 10–100 kHz

(b) Frequency range 15–25 kHz

(c) Frequency range 75–95 kHz

Figure 10: Cable force-loss monitoring by CCD index.

evaluated for cable force-loss monitoring in a lab-scaled test structure.

The implementation of the portable PZT interface was successful in indicating various cable force losses in the lab-scaled tendon anchorage. The EM impedance of the PZT interface was sensitive to the tendon force loss, even when the examined frequency range was smaller than 100 kHz. Both RMSD and CCD damage indicators were successfully employed to quantify the impedance variation due to the loss of cable force. The good monitoring results were achieved not only for the sensitive frequency range but also for the whole measurable frequency band of wireless impedance sensors (i.e., 10–100 kHz). According to the experimental verification, RMSD was chosen as the best damage indicator for cable force-loss monitoring in tendon anchorage using the portable PZT interface. Since the PZT interface is mobile and adaptable to be applied in any existing cable-anchorage connections, it is very promising for practical applications.

Despite the feasibility of the portable PZT interface for the impedance-based cable force monitoring in cable anchorage, further studies are still remaining: (1) the amount of the prestress loss should be quantitatively estimated via the relationships between the prestress loss and the RMSD and CCD indices; (2) since the variation of the contact

stiffness quantitatively represents the cable force loss, the identification of this structural parameter should be carried out; (3) for the practical use of the PZT interface, there is a need to examine the environmental effects on the accuracy of the impedance-based technique.

Conflict of Interests

The authors declare that there is no conflict of interests regarding the publication of this paper.

Acknowledgments

This research was supported by a grant from a Strategic Research Project (Development of Smart Prestressing and Monitoring Technologies for Prestressed Concrete Bridges) funded by the Korea Institute of Construction Technology.

References

[1] H. Sohn, C. R. Farrar, F. M. Hemez, D. D. Shunk, D. W. Stinemates, and B. R. Nadler, "A review of structural health monitoring literature: 1996–2001," Los Alamos National Laboratory Report LA-13976-MS, Los Alamos National Laboratory, Los Alamos, NM, USA, 2003.

[2] C. B. Yun and J. Min, "Smart sensing, monitoring, and damage detection for civil infrastructures," *KSCE Journal of Civil Engineering*, vol. 15, no. 1, pp. 1–14, 2010.

[3] T. H. Yi and H. N. Li, "Methodology developments in sensor placement for health monitoring of civil infrastructures," *International Journal of Distributed Sensor Networks*, vol. 2012, Article ID 612726, 11 pages, 2012.

[4] H. Zui, T. Shinke, and Y. Namita, "Practical formulas for estimation of cable tension by vibration method," *Journal of Structural Engineering*, vol. 122, no. 6, pp. 651–656, 1996.

[5] B. H. Kim and T. Park, "Estimation of cable tension force using the frequency-based system identification method," *Journal of Sound and Vibration*, vol. 304, no. 3-5, pp. 660–676, 2007.

[6] J.-T. Kim, J.-H. Park, D.-S. Hong, H.-M. Cho, W.-B. Na, and J.-H. Yi, "Vibration and impedance monitoring for prestress-loss prediction in PSC girder bridges," *Smart Structures and Systems*, vol. 5, no. 1, pp. 81–94, 2009.

[7] H. Li, J. Ou, and Z. Zhou, "Applications of optical fibre Bragg gratings sensing technology-based smart stay cables," *Optics and Lasers in Engineering*, vol. 47, no. 10, pp. 1077–1084, 2009.

[8] J.-T. Kim, J.-H. Park, D.-S. Hong, and W.-S. Park, "Hybrid health monitoring of prestressed concrete girder bridges by sequential vibration-impedance approaches," *Engineering Structures*, vol. 32, no. 1, pp. 115–128, 2010.

[9] J.-H. Park, J.-T. Kim, D.-S. Hong, D. Mascarenas, and J. Peter Lynch, "Autonomous smart sensor nodes for global and local damage detection of prestressed concrete bridges based on accelerations and impedance measurements," *Smart Structures and Systems*, vol. 6, no. 5-6, pp. 711–730, 2010.

[10] T. C. Huynh, S. Y. Lee, and J. T. Kim, "Wireless structural health monitoring of stay cables under two consecutive typhoons," in *Structural Monitoring and Maintenance*, vol. 1, Techno-Press, 2014.

[11] C. Liang, F. P. Sun, and C. A. Rogers, "Coupled electro-mechanical analysis of adaptive material systems—determination of the actuator power consumption and system energy transfer," *Journal of Intelligent Material Systems and Structures*, vol. 5, no. 1, pp. 12–20, 1994.

[12] G. Park, H. H. Cudney, and D. J. Inman, "Feasibility of using impedance-based damage assessment for pipeline structures," *Earthquake Engineering and Structural Dynamics*, vol. 30, no. 10, pp. 1463–1474, 2001.

[13] A. N. Zagrai and V. Giurgiutiu, "Electro-mechanical impedance method for crack detection in thin plates," *Journal of Intelligent Material Systems and Structures*, vol. 12, no. 10, pp. 709–718, 2001.

[14] S. Bhalla and C. K. Soh, "Structural impedance based damage diagnosis by piezo-transducers," *Earthquake Engineering and Structural Dynamics*, vol. 32, no. 12, pp. 1897–1916, 2003.

[15] Y. Yang, Y. Hu, and Y. Lu, "Sensitivity of PZT impedance sensors for damage detection of concrete structures," *Sensors*, vol. 8, no. 1, pp. 327–346, 2008.

[16] J. T. Kim, W. B. Na, J. H. Park, and D. S. Hong, "Hybrid health monitoring of structural joints using modal parameters and EMI signatures," in *Smart Structures and Materials: Sensors and Smart Structures Technologies for Civil, Mechanical, and Aerospace Systems*, vol. 6174 of *Proceeding of SPIE*, San Diego, Calif, USA, 2006.

[17] D. L. Mascarenas, *Development of an impedance-based wireless sensor node for monitoring of bolted joint preload [M.S. thesis]*, Department of Structural Engineering, University of California, San Diego, Calif, USA, 2006.

[18] F. P. Sun, Z. Chaudhry, C. Liang, and C. A. Rogers, "Truss structure integrity identification using PZT sensor-actuator," *Journal of Intelligent Material Systems and Structures*, vol. 6, no. 1, pp. 134–139, 1995.

[19] T. R. Fasel, H. Sohn, G. Park, and C. R. Farrar, "Active sensing using impedance-based ARX models and extreme value statistics for damage detection," *Earthquake Engineering and Structural Dynamics*, vol. 34, no. 7, pp. 763–785, 2005.

[20] D. L. Mascarenas, M. D. Todd, G. Park, and C. R. Farrar, "Development of an impedance-based wireless sensor node for structural health monitoring," *Smart Materials and Structures*, vol. 16, no. 6, pp. 2137–2145, 2007.

[21] K. D. Nguyen and J. T. Kim, "Smart PZT-interface for wireless impedance-based prestress-loss monitoring in tendon-anchorage connection," *Smart Structures and Systems*, vol. 9, no. 6, pp. 489–504, 2012.

[22] C. Liang, F. Sun, and C. A. Rogers, "Electro-mechanical impedance modeling of active material systems," *Smart Materials and Structures*, vol. 5, no. 2, pp. 171–186, 1996.

[23] K. L. Johnson, *Contact Mechanics*, Cambridge University Press, Cambridge, UK, 1985.

[24] S. Ritdumrongkul, M. Abe, Y. Fujino, and T. Miyashita, "Quantitative health monitoring of bolted joints using a piezoceramic actuator-sensor," *Smart Materials and Structures*, vol. 13, no. 1, pp. 20–29, 2004.

[25] V. Giurgiutiu and A. N. Zagrai, "Embedded self-sensing piezoelectric active sensors for on-line structural identification," *Journal of Vibration and Acoustics*, vol. 124, no. 1, pp. 116–125, 2002.

[26] G. Park, H. Sohn, C. R. Farrar, and D. J. Inman, "Overview of piezoelectric impedance-based health monitoring and path forward," *Shock and Vibration Digest*, vol. 35, no. 6, pp. 451–463, 2003.